Journal of
Applied Crystallography

ISSN 0021-8898

Received 16 August 2006
Accepted 2 January 2007

Core structure of latent heavy-ion tracks in {100} LiF derived by small-angle X-ray scattering

Sameer Abu Saleh and Yehuda Eyal*

Department of Chemistry, Technion – Israel Institute of Technology, Haifa 32000, Israel. Correspondence e-mail: cheyal@techunix.technion.ac.il

Radial electron densities within 27–111 μm-long ion damage trails, 'latent ion tracks', created in {100} LiF by irradiation with GeV Pb and U projectiles, have been derived by means of small-angle X-ray scattering. The tracks exhibit continuous electron density decreases of 49–74% along the centers of their 2.3–3.4 nm-diameter cores. Structural alteration under the intense ion-deposited electronic excitation has been attributed to two successive processes: (*a*) local breakdown of the LiF lattice into fluorine molecules and Li atoms, and (*b*) release of the fluorine gas and of at least a portion of the voluminous Li atoms through the low-density tracks.

1. Introduction

The highly ionic LiF is a prominent nonmetamict crystal, one that does not become disordered by irradiation. Under the impact of a highly energetic heavy ion, however, the deposited intense electronic excitation leads to structural alteration along a narrow track core that surrounds the projectile trajectory. The crystal structure is maintained, as expected, in the peripheral wide track halo. In this region, F-centers are abundant, indicating that the track halo is a strained LiF crystal. The F-center diameter of a track created under linear energy transfer (LET) of 24 keV nm^{-1}, for example, is ~60 nm (Schwartz *et al.*, 1998; Trautmann, Schwartz, Costantini *et al.*, 1998; Trautmann, Toulemonde, Schwartz *et al.*, 2000). As indicated by small-angle X-ray scattering (SAXS) patterns, the track core is a continuous ~3 nm-wide region of modified density (Schwartz *et al.*, 1998; Trautmann, Schwartz, Costantini *et al.*, 1998; Trautmann, Toulemonde, Schwartz *et al.*, 2000). The track exhibits highly enhanced chemical reactivity (Young, 1958; Trautmann, Schwartz & Geiss, 1998), particularly along its core (Abu Saleh & Eyal, 2003), which is an important technological property. Thus, understanding of the fundamental processes in LiF that are initiated by intense electronic excitation is of interest from both academic and practical viewpoints.

In a recent SAXS study, the electron density distribution within 98 μm-long tracks created in {100} LiF by 2.31 GeV Pb ions has been extracted on an absolute scale (Abu Saleh & Eyal, 2005*a*). This study has clearly indicated the importance of ion-induced material expulsion from the track core. We report SAXS-derived track structure from five additional experiments, and discuss the emerging track formation mechanism and the dependence of damage on the deposited ion energy.

2. Specimens and procedures

All substrates were {100} LiF platelets freshly cleaved from a single-crystal block procured from Korth. Specimen and irradiation data are listed in Table 1. All platelets were irradiated at normal beam incidence. A single 111 μm-thick platelet was irradiated half covered by a known energy-degrading Ni foil at GANIL, Caen, and yielded a sample penetrated by 5.97 GeV Pb ions (experiment 1) and a sample penetrated by 4.04 GeV Pb ions (experiment 2). Data of experiment 3 are taken from Abu Saleh & Eyal (2005*a*). In this experiment, the ion beam was stopped in the 167 μm-thick platelet. A single 400 μm-thick platelet was irradiated half covered with an Ni foil at GSI, Darmstadt, and yielded a sample irradiated with 2.64 GeV U ions (experiment 4) and a sample irradiated with 0.50 GeV U ions (experiment 5). All ions were stopped in the substrate. Experiment 6 involved SAXS yields taken as differences of the yields measured in experiments 4 and 5. We view the latter quantities as SAXS yields generated by a 67 μm-thick {100} LiF platelet following irradiation with pseudo-penetrating 2.64 U ions. Here, we assume that the structure of the 27 μm-long end sections of the tracks created in experiment 4 is similar to the structure of the tracks created in experiment 5 (27 μm-long tracks initiated at the platelet surface, see Table 1). After irradiation, the platelets were stored in air at room temperature, mostly in the dark. Platelet thicknesses were determined by X-ray absorption. The areal densities of the tracks, as determined by brief track etching

Table 1
Track data in the examined (100} LiF samples and SAXS-derived track structure parameters (*s* – fractional weight of the hard-cylinder component in the radial electron density function, *f* – fractional electron density deficit along the track center, *R* – mean track radius).

Experiment number	Ion	Ion energy (GeV)	Track length (μm)	Mean LET (keV nm^{-1})	*s*	*f*	*R* (nm)
1	Pb	5.97	111	18.8 ± 0.9	0.83	0.66 ± 0.03	1.17 ± 0.33
2	Pb	4.04	111	22.8 ± 1.6	0.72	0.74 ± 0.03	1.51 ± 0.36
3†	Pb	2.31	98	23.6 + 2.0 − 6.0	0.53	0.49 ± 0.03	1.62 ± 0.30
4	U	2.64	94	27.9 + 2.3 − 6.2	0.60	0.64 ± 0.04	1.69 ± 0.32
5	U	0.50	27	17.9 ± 7.5	0.68	0.50 ± 0.06	1.69 ± 0.32
6‡	U	2.64	67	31.7 ± 0.7	0.60	0.68 ± 0.06	1.69 ± 0.32

† Track data and structure parameters taken from Abu Saleh & Eyal (2005*a*). ‡ Track length and SAXS yields taken as the difference of ion ranges and differences of measured SAXS yields, respectively, in experiments 4 and 5.

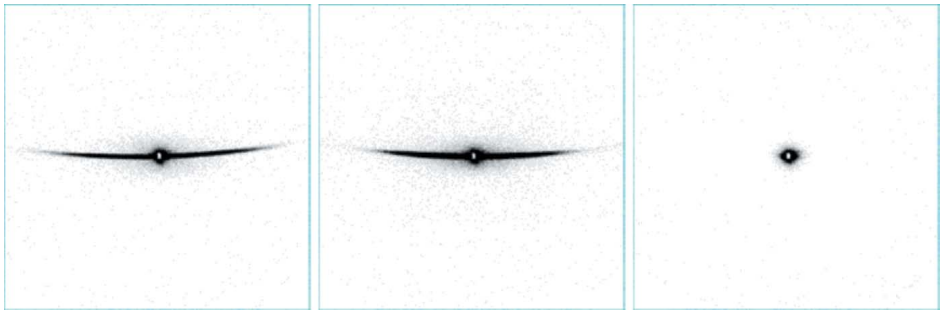

Figure 1
SAXS patterns generated by 111 μm-thick {100} LiF platelets. The platelets were tilted vertically by 30° from a plane perpendicular to the axis of the primary X-ray beam. Left and central panels – scattering patterns generated by platelets following irradiation with 5.97 GeV Pb ions and 4.05 GeV Pb ions, respectively, at normal incidence (see text). Right panel – scattering by a similar but unirradiated control platelet.

combined with high-resolution scanning electron microscopy (see Abu Saleh & Eyal, 2003), were 7.3×10^{10} cm^{-2} in the samples examined in experiments 1 and 2, 4.7×10^{10} cm^{-2} in the sample examined in experiment 3, and 4.0×10^{10} cm^{-2} in the samples examined in experiments 4, 5, and 6 (uncertainties ±3%).

The platelets were examined by SAXS 2–24 months after irradiation. Briefly, the arrangement (Bruker KFF Cu 2 *K*-90) involved a Cu K_α X-ray beam (wavelength λ = 0.1542 nm, beam diameter $\simeq$ 100 μm) and a 1024 × 1024 pixel X-ray detector. The detector covered polar, θ, and azimuthal, φ, scattering angles from ~0.2 to 4.5° and from 0 to 360°, respectively (angular interval per pixel width $w = 1.50 \times 10^{-4}$ rad). The track-originated SAXS yields were obtained by correcting the observed yields for contributions of intact LiF, instrumental background X-radiation, and detector noise. We have neglected interference effects due to 2–3% track overlap, estimated (see Riedel & Spohr, 1979) from the measured areal densities of the tracks and their diameters. Thus, the SAXS intensity was interpreted as the incoherent sum of intensities of individual tracks. The product $P\varepsilon$ (s^{-1}) of the X-ray beam intensity on the target, P (s^{-1}), and the fractional intrinsic efficiency of the X-ray detector, ε ($0 < \varepsilon < 1$), was calibrated by scattering on water (uncertainty 5%) (Abu Saleh & Eyal, 2005*b*), which enabled us to derive absolute SAXS cross sections. The stability of $P\varepsilon$ over time was ensured by frequently monitoring the yield of X rays scattered by a reference carbon glass target.

3. Results

Scattering yields were measured with the track axes tilted away horizontally by α = 0° and vertically by β = 30° from the axis of the primary X-ray beam. As shown by Fig. 1, all SAXS patterns exhibited high anisotropy. Simulations of these experiments (see below and Eyal & Abu Saleh, 2007) have indicated that all registered track-originated events reside in the two mirror-like streaks that extend outward from the center of the X-ray detector and limited to narrow intervals of φ (see Fig. 1), and that each of these events is characterized by $q_r = q$ or $q_r \simeq q$ and $q_z = 0$ or $q_z \simeq 0$, respectively, where $q = (4\pi/\lambda)\sin(\theta/2)$ is the modulus of the scattering vector in the reciprocal space, and q_r and q_z are the moduli of the components of this vector perpendicular and parallel to the track axis, respectively. Thus, the measured two-dimensional yields were translated to convenient one-dimensional yields, $N(q_r)$, by integration of the former yields over φ across the streak and over pixel-wide intervals of θ. One-dimensional yields are displayed in Figs. 2 and 3. The corresponding sequences of average experimental track scattering cross sections are given by

$$\sigma_{\rm exp}(q_r) = \frac{N(q_r)\cos\alpha\cos\beta}{P\varepsilon t D}. \qquad (1)$$

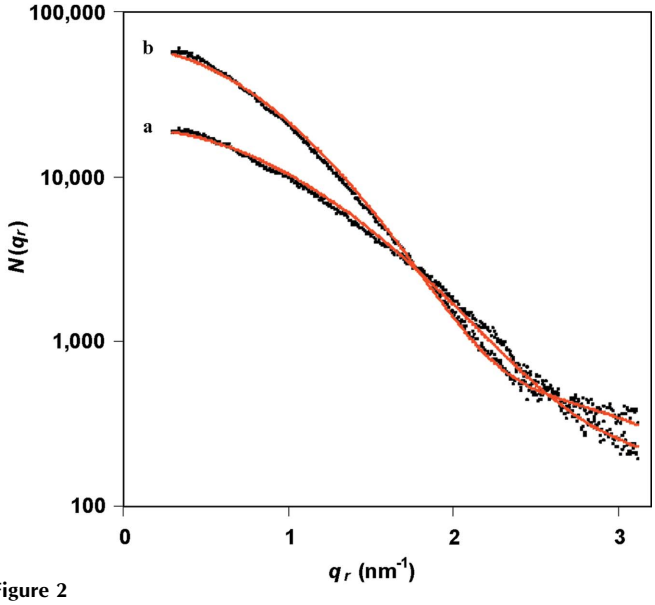

Figure 2
Measured yields (points) of SAXS events generated by ion tracks in 111 μm-thick {100} LiF platelets, $N(q_r)$, *versus* q_r, the modulus of the component perpendicular to the track axis of the scattering vector in the reciprocal space. The curves are model simulations on an absolute scale. Curve a – yields by tracks created by 5.97 GeV Pb ions; curve b – yields by tracks created by 4.05 GeV Pb ions.

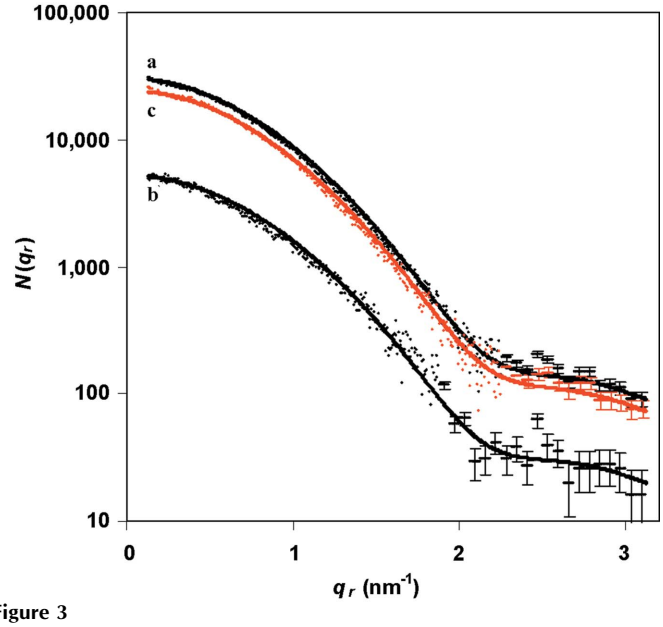

Figure 3
Measured yields (points) of SAXS events generated by ion tracks in {100} LiF platelets, $N(q_r)$, *versus* q_r, the modulus of the component perpendicular to the track axis of the scattering vector in the reciprocal space. The curves are model simulations on an absolute scale. Curve a – yields by 94 μm-long tracks created by 2.64 GeV U ions in a 400 μm-thick platelet; curve b – yields by 27 μm-long tracks created by 0.50 GeV U ions in a 400 μm-thick platelet; curve c – differences of SAXS yields from the two above data sets, representing yields by tracks created by pseudo-penetrating 2.64 GeV U ions through a 67 μm-thick platelet (see text).

Here, D is the areal density of the tracks and t is the duration of the measurement.

We mention that the locations of the local yield maxima along the scattering streaks (Fig. 1) depend upon θ, φ, α and β, which enabled us to assign accurate values for α and β after data collection. In this way, we have avoided errors due to minor misalignment of the LiF platelet during ion irradiation. For example, in experiments 1 and 2 (see Fig. 1), the correct tilting angles were $\alpha = 0.3^\circ$, $\beta = 27.2^\circ$ and $\alpha = 0.0^\circ$, $\beta = 28.1^\circ$, respectively.

4. Track structure model and data analysis

The observed anisotropic SAXS patterns (Fig. 1) indicate the importance of continuous depleted electron density along the tracks. Note that ion-induced compaction of the dense LiF crystal can be safely ruled out. All SAXS patterns also indicate the presence of a damped narrow minimum at $q_r \geq 2.2$ nm^{-1}, which suggests an abrupt change of density at the core circumference. Thus, we have assumed that the track is a depleted columnar structure with largely hard boundaries and cylindrical symmetry. The electron density function was taken to be the same all along the track. Its radial profile, $\rho(r)$, was taken as the sum of contributions of a hard cylinder and a Gaussian with fractional weights s and $1 - s$, respectively ($0 \leq s \leq 1$),

$$\rho(r) = f\rho_0[s\,\delta + (1 - s)\exp(-r^2/R^2)]. \quad (2)$$

Here, ρ_0 is the mean electron density in the LiF matrix, f is the fractional electron density deficit at the track center, R, designated herein as the track radius, is the radial extension of the hard-cylinder component and the e^{-1} radius of the Gaussian component, $\delta = 1$ at $r \leq R$ and $\delta = 0$ at $r > R$. With this function, the sequence of the theoretical one-dimensional track scattering cross sections is given by (Eyal & Abu Saleh, 2007)

$$\sigma(q_r) = \frac{w\lambda L(\pi R^2 f\rho_0 r_e)^2}{\sin\beta\sin\varphi_0 - \sin\alpha\cos\beta\cos\varphi_0} \times \left[2s\frac{J_1(q_r R)}{q_r R} + (1 - s)\exp(-q_r^2 R^2/4)\right]^2. \quad (3)$$

Here $r_e = 2.818 \times 10^{-13}$ cm is the electron scattering length at small θ, L is the track length, φ_0 is the local azimuthal scattering angle at which $q_z = 0$, and J_1 is Bessel function of first order. We have attributed the damping of the minimum in the scattering pattern (Figs. 2 and 3) to dispersion in the track radius. Dispersion is supported by high-resolution microscopy data (unpublished). Thus, the theoretical track scattering cross sections have been derived by numerical integration of equation (3) over a Gaussian distribution of track radii.

Simulated SAXS yields as function of q_r are displayed in Figs. 2 and 3, and the corresponding core structure parameters are listed in Table 1. The derived radial electron density and the derived absolute scattering cross sections of the most probable track created by 4.04 GeV Pb ions are displayed in Figs. 4 and 5, respectively. The highly oscillatory scattering pattern in Fig. 5 is the result of the sharp change of the electron density at a distance of 1.51 nm from the track center (Fig. 4).

5. Discussion

At the time of SAXS measurements, the revealed 2.3–3.4 nm-diameter track cores possessed electron density depletions of 49–74% along the core centers. The specific electron depletion in the most probable track, ∂_e, is obtained by radial integration of equation (2),

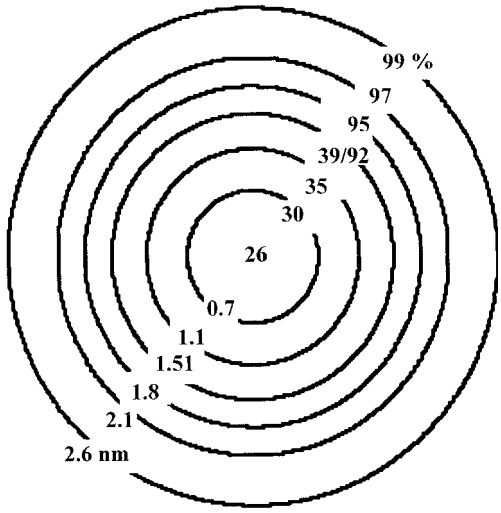

Figure 4
Residual electron density (percent of the matrix electron density) in the most probable 111 µm-long track created in {100} LiF by penetrating 4.05 GeV Pb ions *versus* the radial distance (in nm) from the track center.

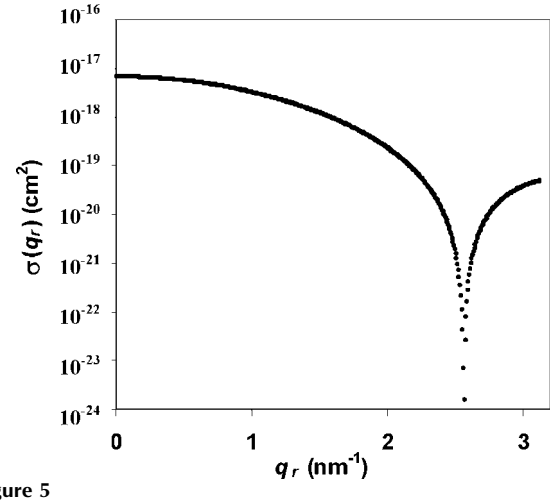

Figure 5
Theoretical SAXS cross sections of the most probable 111 µm-long track created in {100} LiF by a penetrating 4.05 GeV Pb ion. The quantity q_r is the modulus of the radial component of the scattering vector in the reciprocal space.

$$\partial_e = 2\pi f\rho_0\left[s\int_0^R r\,dr + (1 - s)\int_0^\infty \exp(-r^2/R^2)\,r\,dr\right] = f\rho_0\,\pi R^2. \quad (4)$$

The values of ∂_e are 2090, 3900, 2970, 4220, 3300 and 4480 depleted electrons per nanometre of track length in the track cores characterized in experiments 1 through 6, respectively (see Table 1). Thus, material has been undoubtedly removed from the track core. We emphasize that core diameters and electron density deficits have been verified quantitatively and qualitatively, respectively, by transmission electron microscopy (unpublished), but these data are not discussed here.

Because only non-solid alteration products, primarily gases, can gain the mobility necessary for efficient removal from deep beneath the platelet surface, release of radiolytic fluorine gas, produced *via* the reactions LiF (s) $\rightarrow$ Li (g) + F (g) and F (g) $\rightarrow \frac{1}{2}F_2$ (g), has been suggested (Abu Saleh & Eyal, 2005*a*). However, expulsion of Li atoms should be considered as well. Note that the volume occupied by an Li atom in the liquid or solid state is greater by ~33% than the

volume occupied by its precursor, an LiF unit in the crystal [see density of liquid Li in Murday & Cotts (1968)]. Thus, we propose that expulsion of the fluorine gas and at least a portion of the resulting Li atoms must take place. The energy consumed in the above-specified radiolytic process is 7.8 eV per decomposed LiF unit (cohesive energy 10.5 eV, first ionization potential of Li 5.4 eV, electron affinity of F −3.4 eV, and bond energy in F_2 1.6 eV). A possible reaction mechanism is displacive relaxation of a dense cluster of self-trapped excitons (Itoh & Stoneham, 1998). Obviously, efficient removal of Li can be driven by the very high pressure exerted by the atomic and molecular fluorine gas. Moreover, thermal-spike-induced vaporization of LiF along the track core has been predicted by Trautmann, Toulemonde, Schwartz *et al.* (2000). In addition, Li should maintain mobility as a liquid even at a temperature as low as 453 K, which is its solidification temperature. The importance of radiolytic decomposition of LiF under heavy-ion irradiation has been suggested by Schwartz *et al.* (1997), but expulsion of the alteration products has not been considered.

Extracted ∂_e values as a function of the mean ion LET are displayed in Fig. 6. This plot suggests that ion-induced specific electron depletion is nearly proportional to the ion LET. Assuming, for simplicity, the validity of such dependence in the LET range covered by the current data, as shown by the straight line plotted in Fig. 6, the proportionality constant, given by the slope of the line, is 146 (13) keV^{-1}. Thus, species carrying on average 146 electrons are expelled from the track core per 1 keV of deposited ion energy. With this relationship, total material release by a single impinging ion is simply proportional to the full kinetic energy of the ion. Presently, it is difficult to offer a quantitative explanation for this result. Note that a significant portion of the ion energy is deposited initially far away from the projectile trajectory (see Waligorski *et al.*, 1986), so its contribution to damage processes in the track core is expected to be small.

The estimated average numbers of Li atoms and F_2 molecules expelled from the track per 1 keV of deposited ion energy are 3.6 Li atoms and 7.5 F_2 molecules if the track core has been left filled with intact solid Li, and 12.2 Li atoms and 6.1 F_2 molecules if all radiolytic Li has been released from the track. Here, the resulting free volume is 0.20 nm^3 per 1 keV of deposited ion energy. Intermediate release yields fit our analysis if Li that remained in the track has been converted to Li_2O after exposure of the irradiated platelet to air.

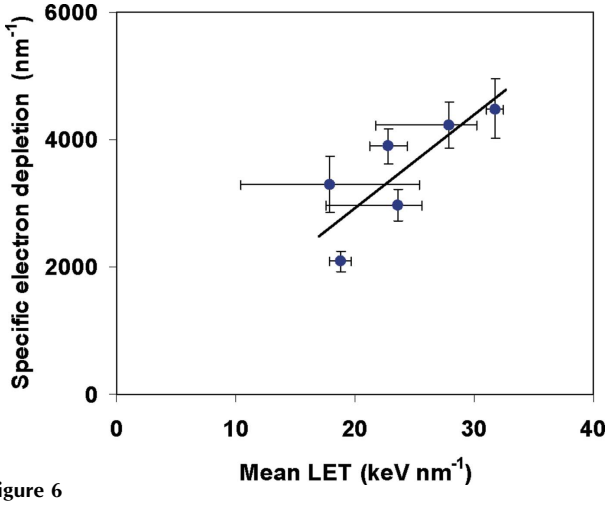

Figure 6
Measured ion-induced specific electron depletion (number of removed electrons per nanometre of track length) *versus* the mean ion LET. The horizontal bars represent dispersion due to variation of the ion LET along the track.

Under this scenario, the quantities of released species range from 5.2 Li atoms and 10.9 F_2 molecules with a resulting free volume of 0.15 nm^3 to 12.1 Li atoms and 6.0 F_2 molecules with a resulting free volume of 0.20 nm^3.

If some of the expelled Li is solidified on the platelet surface, it is possible that the effect contributes to a yet unexplained phenomenon – sizeable swelling of {100} LiF under heavy-ion irradiation – as revealed by means of simple profilometry (Trautmann, Toulemonde, Costantini *et al.*, 2000). With the swelling data reported by Trautmann Toulemonde, Costantini *et al.* (2000), we find that under mean LET ranging from 17.3 to 24.6 keV nm^{-1}, essentially constant specific swelling volume has been measured, with a mean value of 0.10 (0.02) nm^3 per 1 keV of deposited projectile energy. Here, the swelling data were derived from nine experiments that involved irradiations with highly energetic Au, Pb, Bi and U ions. This result is compatible with the release of 8.2 (1.7) Li atoms per 1 keV of deposited ion energy, if at the time of profilometry analysis the deposited material has been Li_2O.

Two other known material expulsion processes that involve ejection of solid or of readily solidified material from {100} LiF under heavy-ion irradiation are hillock formation (Müller *et al.*, 2002) and stoichiometric sputtering of Li and F atoms (Toulemonde *et al.*, 2002). Both involve release of relatively minute quantities of material. The origin of the former process is yet unclear. The second process indicates release in excess of thermally activated sputtering (Toulemonde *et al.*, 2002). Here, release that is driven by a vapor phase has been invoked (Toulemonde *et al.*, 2002). Thus, it is possible that these two processes are small side effects of the phenomenon considered in the present research.

6. Summary and conclusions

Significant electron density decreases along the ∼3 nm-wide cores of tracks created in {100} LiF by highly energetic Pb and U ions have been revealed by SAXS. It has been proposed that structural alteration occurs *via* a two-stage process which is initiated by the local and intense ion-deposited electronic excitation. The first stage involves disintegration of the LiF lattice into Li and F atoms, with the latter atoms creating F_2 molecules. The second stage involves release of the fluorine gas and of at least a portion of the voluminous Li atoms through the low density tracks. It is possible that solidification of removed Li on the surface of the irradiated platelet contributes significantly to the yet unexplained sizeable swelling of {100} LiF under irradiation with highly energetic heavy ions. The predicted chemical composition of the track core – a region filled with intact lithium or containing significant free volume and Li_2O – may explain the proven great reactivity of this central region of the track.

The authors thank Drs C. Trautmann and K. Schwartz, GSI, Darmstadt, and Dr M. Toulemonde, GANIL/CIRIL Caen, for performing the ion irradiations. This work was supported by grant 23/03 of the Israel Science Foundation, and by the S. Langberg Nuclear Research Fund at the Technion.

References

Abu Saleh, S. & Eyal, Y. (2003). *Nucl. Instrum. Methods Phys. Res. Sect. B*, **209**, 113–117.
Abu Saleh, S. & Eyal, Y. (2005*a*). *Nucl. Instrum. Methods Phys. Res. Sect. B*, **230**, 246–250.

Abu Saleh, S. & Eyal, Y. (2005*b*). *Nucl. Instrum. Methods Phys. Res. Sect. B*, **236**, 81–87.
Eyal, Y. & Abu Saleh, S. (2007) *J. Appl. Cryst.* **40**, 71–76.
Itoh, N. & Stoneham, A. M. (1998). *Nucl. Instrum. Methods Phys. Res. Sect. B*, **146**, 362–366.
Müller, C., Cranney, M., El-Said, A., Ishikawa, A., Iwase, M., Lang, M. & Neumann, R. (2002). *Nucl. Instrum. Methods Phys. Res. Sect. B*, **191**, 246–250.
Murday, J. S. & Cotts, R. M. (1968). *J. Chem. Phys.* **46**, 4938–4945.
Riedel, C. & Spohr, R. (1979). *Radiat. Eff.* **42**, 69–75.
Schwartz, K., Trautmann, C., Steckenreiter, T., Geiss, O. & Kramer, M. (1998). *Phys. Rev. B*, **58**, 11232–11240.
Schwartz, K., Wirth, K., Trautmann, C. & Gruner, F. (1997). *Phys. Rev. B*, **56**, 10711–10714.
Toulemonde, M., Assmann, W., Trautmann, C. & Gruner, F. (2002). *Phys. Rev. Lett.* **88**, 057602-1–057602-4.
Trautmann, C., Schwartz, K., Costantini, J. M., Steckenreiter, T. & Toulemonde, M. (1998). *Nucl. Instrum. Methods Phys. Res. Sect. B*, **146**, 367–378.
Trautmann, C., Schwartz, K. & Geiss, O. (1998). *J. Appl. Phys.* **83**, 3560–3564.
Trautmann, C., Toulemonde, M., Costantini, J. M., Grob, J. J. & Schwartz, K. (2000). *Phys. Rev. B*, **62**, 13–16.
Trautmann, C., Toulemonde, M., Schwartz, K., Costantini, J. M. & Müller, A. (2000). *Nucl. Instrum. Methods Phys. Rev. B*, **164–165**, 365–376.
Waligorski, M. P. R., Hamm, R. N. & Katz, R. (1986). *Nucl. Tracks Radiat. Meas.* **11**, 309–319.
Young, D. A. (1958). *Nature* (*London*), **182**, 375–377.